# Size-dependent line broadening in the emission spectra of single GaAs quantum dots: Impact of surface charge on spectral diffusion

Neul Ha,[1,2] Takaaki Mano,[1] Ying-Lin Chou,[3] Yu-Nien Wu,[3] Shun-Jen Cheng,[3] Juanita Bocquel,[4] Paul M. Koenraad,[4] Akihiro Ohtake,[1] Yoshiki Sakuma,[1] Kazuaki Sakoda,[1] and Takashi Kuroda[1,2,*]

[1]*National Institute for Materials Science, 1-1 Namiki, Tsukuba 305-0044, Japan*

[2]*Graduate School of Engineering, Kyushu University, NIMS, Tsukuba 305-0044, Japan*

[3]*Department of Electrophysics, National Chiao Tung University, Hsinchu 30050, Republic of China*

[4]*Eindhoven University of Technology, 5600 MB Eindhoven, The Netherlands*

(Received 9 April 2015; revised manuscript received 19 July 2015; published 10 August 2015)

Making use of droplet epitaxy, we systematically controlled the height of self-assembled GaAs quantum dots by more than one order of magnitude. The photoluminescence spectra of single quantum dots revealed the strong dependence of the spectral linewidth on the dot height. Tall dots with a height of ∼30 nm showed broad spectral peaks with an average width as large as ∼5 meV, but shallow dots with a height of ∼2 nm showed resolution-limited spectral lines ($\leqslant$120 $\mu$eV). The measured height dependence of the linewidths is in good agreement with Stark coefficients calculated for the experimental shape variation. We attribute the microscopic source of fluctuating electric fields to the random motion of surface charges at the vacuum-semiconductor interface. Our results offer guidelines for creating frequency-locked photon sources, which will serve as key devices for long-distance quantum key distribution.

DOI: 10.1103/PhysRevB.92.075306 PACS number(s): 78.67.Hc, 78.55.Cr, 73.21.La

## I. INTRODUCTION

Numerous photonic applications using semiconductor quantum dots rely on the discrete and delta-function-like density of states [1]. However, various single-dot spectroscopy studies have confirmed significant line broadening in the photoluminescence spectra, which is normally much broader than the transform limited width determined by the spontaneous emission rate. The line broadening mechanism is commonly attributed to spectral diffusion, where the transition frequency randomly changes through the fluctuation of a local electric field in the vicinity of dots [2–5]. The fluctuating spectral line becomes integrated into a relatively broad peak thanks to the long time scales of signal integration compared with those of environmental motion.

Some progress has been made in studying the short time scale dynamics of the spectral fluctuation. Photon correlation measurement can elucidate spectrally diffusive photoluminescence with subnanosecond characteristic times [6,7]. The correlation functions routinely show monoexponent decays, which implies efficient coupling between a single dot and a small number of environment configurations. In contrast, resonant fluorescence measurements reveal broadband noise spectra in the 0.1 Hz to 100 kHz range, where contributions can be expected from a large number of environment configurations [8]. Photon counting statistics of resonant fluorescence further reveal the Gaussian distribution of the random environmental shifts, which might be a consequence of the central limit theorem adopted for a large ensemble [9]. By contrast, high-resolution Fourier transform measurement confirms a motionally narrowed Lorentzian line shape associated with rapid environmental fluctuation [10]. More recent work on field-effect devices identifies charge traps at the barrier/well interface [11] or impurity centers [12] as a dominant field source. Thus the time scales and magnitudes of spectral diffusion vary greatly depending on the sample and the measurement conditions. We still lack a global understanding of the microscopic mechanism of spectral diffusion, however, it is needed for developing frequency-locked photon sources as basic elements in long-distance quantum key distribution, e.g., quantum repeaters for extending the key transmission distance.

In this work, we experimentally analyze the dependence of quantum dot morphology on the environment-mediated spectral broadening. For this purpose, we focus on GaAs quantum dots grown by droplet epitaxy, which enables us to continuously control the quantum dot height by more than one order of magnitude. The morphology tunability contrasts with that of traditional quantum dot growth using the Stranski-Krastanow mode, where the dot profile is essentially fixed by strain relaxation and surface energies. The spectral linewidth of a single dot emission depends strongly on the dot height. The measured height dependence agrees with that of Stark coefficients along the growth direction (normal to the sample surface). We attribute the source of the electric field fluctuation to the change in the microscopic configuration of surface charges at the vacuum-semiconductor interface [13,14]. Thus morphology engineering is an alternative route to achieving narrower emitter linewidths without the need for feedback techniques to suppress spectral fluctuation [15,16].

## II. EXPERIMENTAL PROCEDURE

### A. Sample preparation

GaAs quantum dots were self-assembly grown in $Al_{0.3}Ga_{0.7}As$ by droplet epitaxy on semi-insulating GaAs(100) substrates [17,18]. These dots are free from strain thanks to the negligible lattice mismatch between GaAs and $Al_{0.3}Ga_{0.7}As$. After the growth of a 100-nm $Al_{0.3}Ga_{0.7}As$ layer, different amounts of gallium ($\theta_{Ga}$) with 1.5, 2, 3, 5, 7.5, or 10 monolayers

*kuroda.takashi@nims.go.jp

 ©2015 American Physical Society

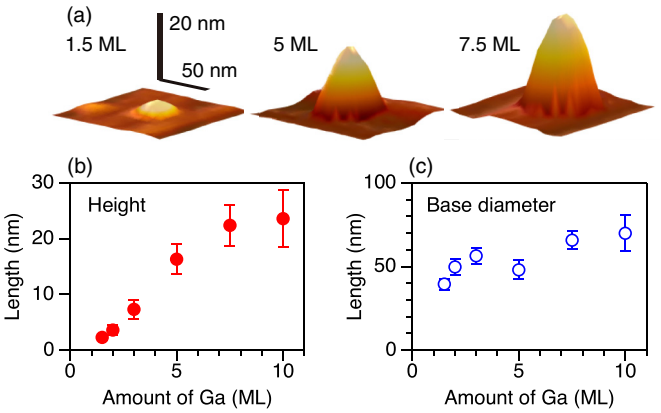


FIG. 1. (Color online) (a) Three-dimensional AFM images for typical GaAs quantum dots grown by droplet epitaxy on $Al_{0.3}Ga_{0.7}As(100)$ with different amounts of gallium deposition $\theta_{Ga}$. (b) and (c) The average height and the base diameter, respectively, of quantum dots as a function of $\theta_{Ga}$. The error bars represent the standard deviation of profile statistics.

(ML) were deposited at 0.5 ML/s and 200 °C. This step enabled the formation of gallium droplets. Then, an $As_4$ flux was supplied at $2.5 \times 10^{-4}$ Torr and 200 °C, and the gallium droplets were fully crystalized to GaAs dots. Note that the $As_4$ flux was roughly two orders of magnitude higher than that used for the self-assembly of quantum ring structures [19].

After the dots were grown, the sample was annealed at 400 °C *in situ* (under a weak $As_4$ supply) for 10 min, and partially capped with a 20-nm $Al_{0.3}Ga_{0.7}As$ layer. The temperature was then increased to 580 °C, while the capping continued with a 30-nm $Al_{0.3}Ga_{0.7}As$ layer followed by a 10-nm GaAs layer. GaAs dots on a 2-ML $Al_{0.3}Ga_{0.7}As$ layer were additionally grown on the top of samples for atomic force microscopy (AFM) analysis. Finally, rapid thermal annealing was carried out at 800 °C for 4 min in a $N_2$ atmosphere. All the samples with different amounts of $\theta_{Ga}$ exhibited well-defined dots; see AFM top views in Appendix A. The dot density depended only slightly on $\theta_{Ga}$ from $1.8 \times 10^{10}$ $cm^{-2}$ (1.5 ML) to $1.2 \times 10^{10}$ $cm^{-2}$ (10 ML). Thus we assume that the volumes per dot are nearly proportional to $\theta_{Ga}$.

### B. Optical setup

We used a continuous-wave laser that emitted at a wavelength of 532 nm as an excitation source. The laser illumination generated photocarriers in the $Al_{0.3}Ga_{0.7}As$ barrier. The excitation polarization was set to be linear in order to avoid a spectral shift of nuclear origin [20,21]. Our confocal setup combined an objective lens with a numerical aperture of 0.55 and a hemispherical solid immersion lens (SIL) with a refractive index of two. The use of the high-index SIL enabled us to reduce the focusing diameter to ~0.5 $\mu$m [22], where approximately 25 dots were inside the spot. The excitation density was kept sufficiently low so that the carrier population was less than 0.5, and the influence of strong optical injection on line broadening was fairly removed. Photoluminescence signals were fed into a spectrometer of a 50-cm focusing length, and analyzed with a full width at half maximum

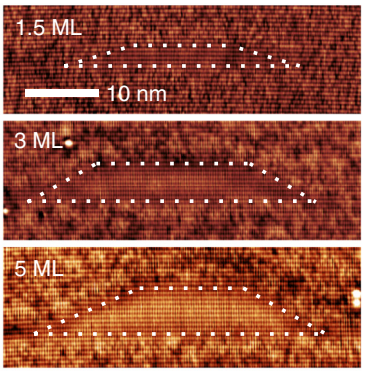


FIG. 2. (Color online) Cross-sectional STM topography images of GaAs quantum dots capped with $Al_{0.3}Ga_{0.7}As$. The white dotted lines are guides to the eye that highlight the dot-barrier interface.

(FWHM) resolution of 120 $\mu$eV. All the experiments were carried out at 10 K.

## III. RESULTS AND DISCUSSIONS

### A. Morphology analysis

Figure 1(a) shows AFM three-dimensional views whose height increases significantly with the amount of $\theta_{Ga}$. Figures 1(b) and 1(c) show the average dot height and the base diameter, respectively, which were determined by statistical analysis. When the amount of $\theta_{Ga}$ was increased from 1.5 to 10 ML, the dot height increased from 2.3 (±0.5) to 24 (±5) nm, i.e., by a factor of ten. In contrast, the base size increased only by a factor of less than two. Thus the dot height increased considerably as the dot volume increased, while the base size remained almost unchanged. The mechanism responsible for the volume-dependent aspect ratio is explained in terms of the two-step crystallization process involved in droplet epitaxy, see Appendix A.

Figure 2 shows the morphology of GaAs quantum dots capped with an $Al_{0.3}Ga_{0.7}As$ matrix that was measured using cross-sectional scanning tunneling microscopy (X-STM) [23]. They have a truncated pyramidal shape, which agrees with the AFM cross-sections of uncapped dots. Thus GaAs dots are embedded in $Al_{0.3}Ga_{0.7}As$ while maintaining their original shape. This is due to the small diffusion length of aluminum atoms, which further gives rise to the formation of a distinct dot-barrier interface free from composition mixing [24]. This observation is in stark contrast to commonly studied InAs/GaAs dot systems, where indium atoms diffuse efficiently, and composition mixing leads to the deformation of dots with capping. This shape conservation allows the determination of the shape of embedded dots from AFM measurements of free-standing references. The X-STM image reveals a clear interface without any dislocations, which indicates a high crystal quality in the present samples.

### B. Photoluminescence spectra

Figure 3(a) shows the spectra of a large ensemble of quantum dots. They were measured using long-focus optics. The spectral peaks at ~1.51 eV originate from impurity-bound excitons in the GaAs substrate. Signals associated with

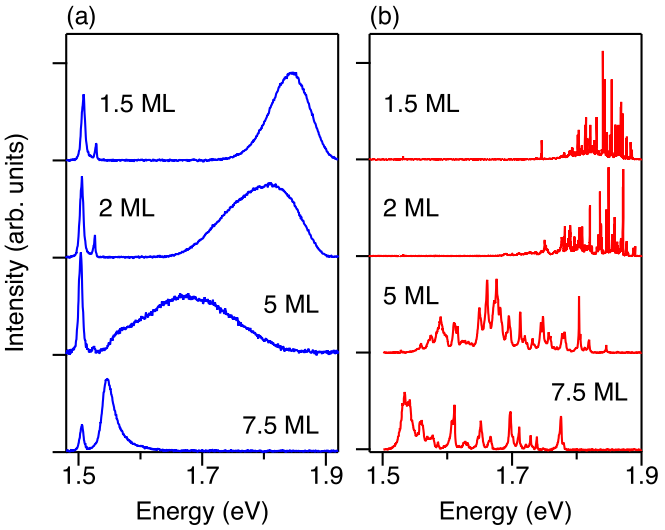


FIG. 3. (Color online) Comparison of (a) photoluminescence spectra of a large ensemble of GaAs quantum dots, and (b) those of a small number of dots selected using a micro-objective setup.

quantum dots are observed at 1.85, 1.8, and 1.67 eV in the 1.5-, 2-, and 5-ML samples, respectively. The emission peak, therefore, shifts to a lower energy side with increasing droplet volume. The 7.5 ML sample shows a relatively narrow peak at 1.55 eV, which is close to the bulk band gap of GaAs.

Figure 3(b) shows the emission spectra of a small ensemble of quantum dots that were spatially selected using a micro objective setup. The spectra of both the 1.5- and 2-ML samples consist of sharp lines, whose linewidths are close to, or less than, the instrumental response of our spectrometer. There are around 70 spectral lines, which is approximately three times the expected number of dots inside a focusing spot. The discrepancy is reasonable because each dot is able to generate three to four emission lines through the formation of different types of charged/neutral exciton complexes [25].

In contrast, the 5- and 7.5-ML samples exhibit relatively broad peaks that dominate the emission signals at energies below 1.75 eV. Note that a few sharp lines are also observed at energies higher than 1.8 eV, as found with the spectral lines of the 1.5 and 2 ML samples. Thus the broad peaks for low-energy dots and narrow peaks for high-energy dots are not sample-specific signatures, but universal size-dependent behaviors.

Figure 4 shows linewidth statistics as a function of emission energy. Here, we evaluate the FWHM of all the spectral lines by fitting without distinguishing between the neutral and charged transitions. Such treatment is sufficient to clarify the general trend of size-dependent broadening, since the difference between the neutral and charged exciton linewidths is much smaller than the observed dot-to-dot variation, as confirmed previously [26]. The compiled statistics demonstrate a clear correlation between line broadening and emission energy. The smooth transition over the data points of different samples confirms that the linewidth reaches several meV for tall dots, and decreases monotonically to the resolution limit with decreasing dot height. The similar linewidth dependence on emission energies has recently been reported for polar nitride quantum dots [27].

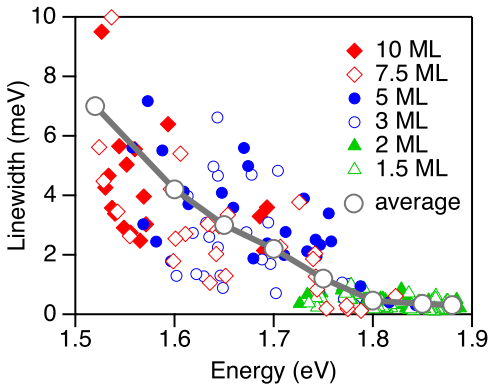


FIG. 4. (Color online) Dependence of the linewidth of the spectral line on the emission energy. Gray open circles are the values averaged over all the spectral lines in each sample.

### C. Environment-induced line broadening

The effect of the environment on spectral shifts is twofold. First, hyperfine coupling between an electron and nuclei induces the Overhauser field, which acts as an effective magnetic field in the tens of millitesla range [28]. Second, a charge distribution in the vicinity of dots induces a local electric field. However, the effect of nuclear fluctuation on line broadening is considered to be negligible at least in the present samples, because a typical value for a nuclear field is 10 mT, which corresponds to a spectral shift of 0.25 $\mu$eV for GaAs [21]. This is much smaller than the observed linewidth, which reaches several meV. Thus the following discussion deals only with the effect of electric field fluctuation on line broadening.

A local electric field has various microscopic origins. A common example of a field source is charge particles trapped in impurities or defects. However, their densities are normally very low in samples grown with molecular beam epitaxy (MBE, $\sim 10^{14}$ cm$^{-3}$). Hence it is difficult for the bulk impurities or defects to realize line broadening that are comparable to the measured spectra, as also discussed later. Despite the charging and discharging of trapping centers close to dots, here we propose the fluctuation of charge carriers trapped by the vacuum-semiconductor interface as a field source.

The formation of surface states, which trap charge carriers, is linked to the presence of electronically active defects at the vacuum-semiconductor interface [29]. It is known that the surface state density depends on orientations and chemical treatments, and reaches $10^{14}$ cm$^{-2}$ for a naturally oxidized GaAs(100) surface [30]. Charge carriers are efficiently trapped by the surface states, and induce a local electric field normal to the surface on average. The phenomenon also serves as the origin of band bending and Fermi-level pinning [31]. When the sample is optically excited, some of the photoinjected carriers recombine with surface charges, and others occupy different surface states. Consequently, the microscopic charge arrangement changes randomly, which gives rise to field fluctuation and spectral broadening through time integration. The effect is orientation dependent, and taller dots become more sensitive to the induced field.

### D. Size-dependent Stark coefficients

Qualitative explanation of the measured line broadening is based on the derivation of Stark coefficients and the simulation of field fluctuation. The Stark shift $E_S$ of a single-particle level is described by the second-order perturbation of the interaction Hamiltonian, i.e.,

$$E_S = \sum_{n\geqslant 2} \frac{|\langle\psi_1|eFz|\psi_n\rangle|^2}{E_1 - E_n} = (eF)^2 \sum_{n\geqslant 2} \frac{Z_{1n}^2}{E_1 - E_n}, \qquad (1)$$

where $F$ is an electric field, $E_1$ and $E_n$ are the single-particle eigenenergies of the ground and the $n$th excited states, respectively, and $Z_{1n} = |\langle\psi_1|z|\psi_n\rangle|$ is a dipole moment along a direction parallel to the field. The above equation demonstrates the size dependence of Stark shifts, where the dipole moment is proportional to the confinement length $L$, the energy denominator is scaled by $(\pi^2\hbar^2/2m)L^{-2}$, hence the Stark coefficient is enhanced as the fourth power of the effective dot size along a built-in field, see Appendix B for calculation details.

Figure 5(a) shows the field dependence of spectral shifts calculated for a 12-nm-high GaAs dots. The lines show the analytic dependence for a model based on infinite-potential quantum boxes with $m_e^*(m_h^*) = 0.067\,(0.5)$, and the circles are the results obtained with a more precise model, which takes account of the finite GaAs/$Al_{0.3}Ga_{0.7}$As potential and the effect of valence-band mixing in terms of four-band $\mathbf{k}\cdot\mathbf{p}$ perturbation. Both models exhibit parabolic dependence, as expected. Enhanced shifts in the finite-potential dot with respect to the infinite-potential dot arise due to the extended wave function. These results imply that an energy shift as large as 1 meV, which is a typical linewidth in the measured spectra, requires a field strength of the order of 10 kV/cm, which is expected at a position only ~8 nm from a point charge. Accompanying impurities or defects in such close proximity to dots is fairly uncommon for MBE grown samples. This is why we have excluded bulk trapping centers and proposed surface charges as a field source.

### E. Simulation of field fluctuation

We evaluate the field fluctuation using a Monte Carlo simulation, where an electric field is induced by randomly positioned charge particles in a flat layer. Figure 5(b) shows the field strength distribution at a point 60 nm from the surface (dielectric constant $\epsilon = 13$). This condition reproduces the geometry of our structure. We found that the field changes randomly with different charge arrangements. The statistics yields a mean field strength $F_0$ of 7 kV/cm and a standard deviation of 1.4 kV/cm for a charge density of $1 \times 10^{11}$ cm$^{-2}$. The validity of this simulation is confirmed by the agreement between the observed mean strength and the value predicted for a uniform charge sheet, $F_z = \sigma/2\pi\epsilon\epsilon_0 \approx 6.97$ kV/cm, where $\sigma$ denotes a charge density. We performed the simulation for different values of $\sigma$, and found that the magnitude of field fluctuation $\Delta F$ is nearly proportional to $\sqrt{\sigma}$, see Appendix C for discussion about the underlying mechanism.

We assume that $\Delta F$ transfers proportionally to line broadening $\Delta E_S$, i.e.,

$$\Delta E_S \approx \Delta F \left.\frac{\partial E_S(F)}{\partial F}\right|_{F=F_0} = E_S(F_0)\frac{2\Delta F}{F_0}. \qquad (2)$$

The substitution of Eq. (1) into Eq. (2) yields the line broadening dependence on the transition energy of dots, see Appendix B for simulation details. Figure 6 compares the experimental linewidths and the calculated spectral fluctuation for different charge densities. There is fairly good agreement between the experimental widths and calculated broadening when the charge density is of the order of $10^{11}$ cm$^{-2}$, which is a reasonable value [32].

Note that the lower bound of the measured linewidths in Fig. 6 is limited by our spectrometer resolution, though a previous investigation on similar dot systems using a

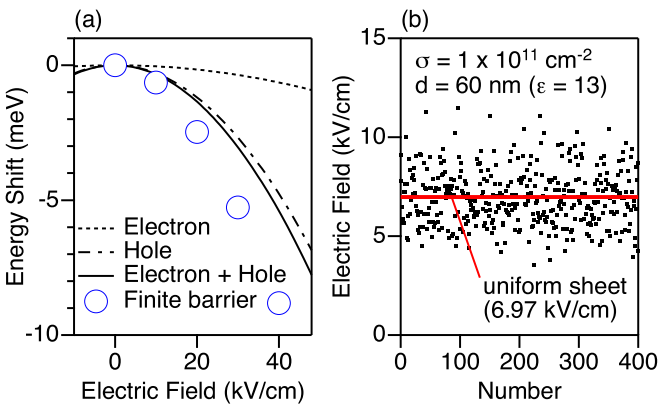


FIG. 5. (Color online) (a) Calculated Stark shift for a 12-nm-high GaAs quantum box surrounded by an infinite barrier (lines) and a finite barrier (open circles) as a function of a vertical field. (b) Monte Carlo simulation for electric fields induced by randomly positioned surface charges with a density of $1 \times 10^{11}$ cm$^{-2}$ at a point 60 nm from the charge layer. The red line shows a field strength induced with a uniform charge sheet.

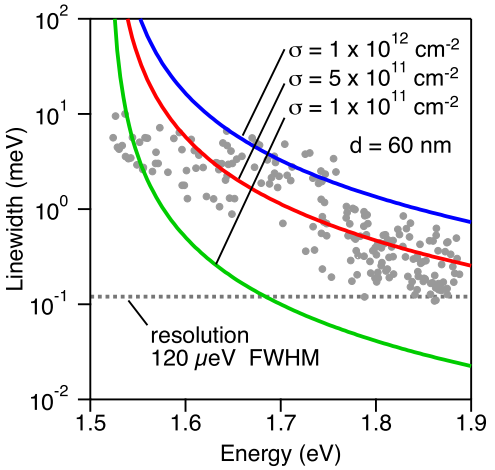


FIG. 6. (Color online) Calculated energy fluctuations due to randomly positioned surface charges with different densities of $1 \times 10^{11}$, $5 \times 10^{11}$, and $1 \times 10^{12}$ cm$^{-2}$. The experimentally measured linewidths are also indicated by the gray points, which are equivalent to the data points shown in Fig. 4.

higher-resolution spectrometer revealed the linewidths as large as a few tens of $\mu$eV at wavelengths around 1.8 eV [18]. Note also that the model curves in Fig. 6 exceed the measured linewidths at low energies. These inconsistent asymptotes are attributed to the fact that the present model ignored the effect of Coulomb binding. The quantum confined Stark shifts are associated with the wave-function separation between electrons and holes. Coulomb attraction would inhibit such separation, and suppress energy shifts. The upper bound of line broadening is therefore roughly provided by the exciton binding energies, which were predicted to be a few tens of meV for GaAs/$Al_{0.3}Ga_{0.7}As$ dots [25].

## IV. CONCLUSIONS

Spectral diffusion in the photoluminescence of single quantum dots is an interesting phenomenon that bridges microscopic random dynamics and macroscopic optical response. Here we studied morphologically controlled GaAs quantum dots grown by droplet epitaxy to understand the source of environmental fluctuation, and demonstrated the impact of fluctuating surface charges on dot line broadening.

From a technological point of view, however, the line broadening phenomenon is unfavorable for practical applications of quantum dots to photon emitting devices. The present results suggest several ways to engineer spectral broadening. First, we expect to suppress line broadening by creating dots with a sufficiently low aspect ratio that are robust as regards a random electric field normal to surface. Second, we expect to achieve narrower spectra by embedding dots more deeply in the barrier matrix, where the effect of random charges at the surface would be effectively smoothed out. Line broadening is expected to decrease with the inverse of the dot-surface distance, see Appendix C for the simulation result. Finally, the use of a substrate with a chemically stable surface, such as a gallium terminated (111)A surface [33–35], and/or defect passivation technologies [30,32,36] are another potential route by which to reduce surface charge fluctuation.

*Note added:* Study on the growth mechanism of height-controlled quantum dots by droplet epitaxy has recently been reported [37].

## ACKNOWLEDGMENTS

This work was partially supported by Grant-in-Aid from Japan Society for the Promotion of Science (KAKENHI Grants No. 24510145 and No. 25390011). S.J.C. acknowledges support from the National Science Council of Taiwan (Contract No. NSC-102-2112-M-009-009-MY2).

## APPENDIX A: MECHANISM FOR THE VOLUME-DEPENDENT ASPECT RATIO OF GAAS QUANTUM DOTS

Figure 7 shows the AFM top view of each sample with different amounts of gallium supply. The dot density is estimated to be 1.8, 1.9, 1.3, 1.2, 1.1, and 1.2 $\times$ $10^{10}$ $cm^{-2}$ for samples with gallium supply of 1.5, 2, 3, 5, 7.5, and 10 ML, respectively. Figure 8(a) shows the AFM cross-section normal to the [1–10] in-plane direction for a typical dot in each sample.

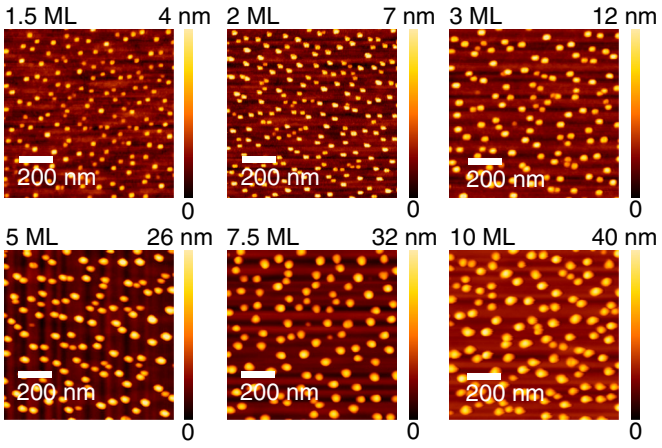


FIG. 7. (Color online) Atomic force microscopy images of GaAs quantum dots grown on $Al_{0.3}Ga_{0.7}As(100)$ by droplet epitaxy for different amounts of gallium supply; 1.5, 2, 3, 5, 7.5, and 10 ML. Note that [1-10] ([110]) in-plane axis is oriented horizontally (vertically).

When the gallium supply is increased from 1.5 to 7.5 ML, the dot height increases by a factor of ten, but the lateral size increases only by a factor of less than two. Thus the aspect ratio (vertical to horizontal ratio) depends strongly on the droplet volume.

Figure 8(b) shows a mechanism that is possibly responsible for the volume dependent aspect ratio. Liquid gallium droplets are expected to have nearly the same aspect ratio regardless of the volume. When intense $As_4$ is supplied, the crystallization of gallium into GaAs occurs initially at the edges of the droplets, where Ga and As atoms meet with a higher probability on the surface. Then, side slopes emerge and grow at the droplet edges. With small droplets, crystallization is complete once shallow side slopes are formed. With large droplets, crystallization continues until stable facets (most probably {111}) appear. Consequently, large droplets become tall dots with a steep profile. Note that side-slope formation allows the self-assembly of quantum rings for a sufficiently low $As_4$ flux [19]. The detail of growth kinetics responsible for the volume-dependent aspect ratio will be described in a forthcoming article [37].

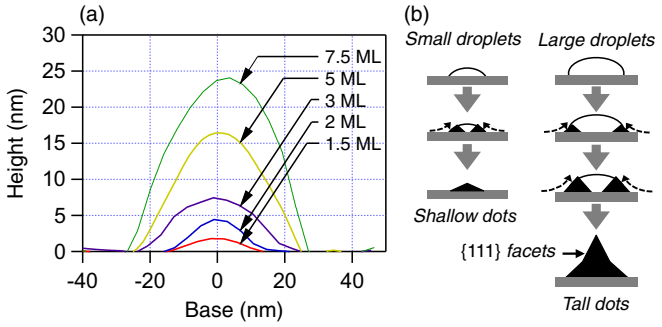


FIG. 8. (Color online) (a) Cross-sectional profiles normal to [1–10] for typical GaAs quantum dots grown on $Al_{0.3}Ga_{0.7}As(100)$. (b) Schematic drawing of a possible growth mechanism for GaAs dots on a (100) surface by droplet epitaxy.

## APPENDIX B: PERTURBATIVE CALCULATION OF STARK SHIFTS AND SIZE-DEPENDENT SPECTRAL BROADENING

The photoluminescence energy of an exciton confined in a dot is given by $E_{\rm PL} = E_g^{\rm bulk} + E_1^e + E_1^h - V_{eh}$, where $E_g^{\rm bulk} = 1.52$ eV is the energy gap of bulk GaAs, $E_1^{e(h)}$ is the energy of the lowest bound state of a single electron (hole) in the dot, and $V_{eh}$ is the magnitude of the direct Coulomb interaction between the electron and hole in the exciton. In the second-order perturbation theory, the energies of the lowest single particle states under a constant electric field $F$ along $z$ axis is approximated to $E_n^\nu \approx E_n^{\nu(0)} + E_n^{\nu(2)}$, where $\nu = e/h$ denotes the kind of particles, i.e., an electron or a hole, and $E_n^{\nu(i)}$ is the $i$-order correction to the energy. In the hard-wall quantum box model, the unperturbed bound state energies are given by

$$E_n^{\nu(0)} = E_{n_x,n_y,n_z}^{\nu} = \frac{\pi^2\hbar^2}{2m_\nu}\left(\frac{n_x^2}{L_x^2} + \frac{n_y^2}{L_y^2} + \frac{n_z^2}{L_z^2}\right), \qquad \text{(B1)}$$

where $L_x$, $L_y$, and $L_z$ are the side lengths of the quantum box, $m_\nu$ are the effective masses of particles, and the composite indices $n = 1,2,3,\ldots$ represent the sets of quantum numbers $(n_x,n_y,n_z)$ with $n_x,n_y,n_z = 1,2,3,\ldots$ following the order of energy. Neglecting the weak field dependence of $V_{eh}$, the field-dependent Stark shift $E_S^X$ is given by

$$E_S^X \approx E_1^{e(2)} + E_1^{h(2)} = \sum_{\nu=e,h}\sum_{n\geqslant 2}\frac{\left|\langle\psi_1^\nu|eFz_\nu|\psi_n^\nu\rangle\right|^2}{E_1^{\nu(0)} - E_n^{\nu(0)}}, \qquad \text{(B2)}$$

where $\psi_n^\nu$ is the wave function of the $n$ state of an electron or a hole. Using the explicit form of $\psi_n^\nu$ given in Ref. [38], we reach,

$$E_S^X = -\left(\frac{512}{243\pi^6}\right)\left(\frac{m_e + m_h}{\hbar^2}\right)e^2F^2L_z^4. \qquad \text{(B3)}$$

When the electric field fluctuates by $\Delta F$ around a mean value of $F_0$, the Stark shifted spectral line is integrated into a broad peak with a linewidth of $\Delta E_S^X$, which is approximated as

$$\Delta E_S^X \approx \Delta F\left.\frac{\partial E_S^X(F)}{\partial F}\right|_{F=F_0}$$

$$= \left(\frac{1024}{243\pi^6}\right)\left(\frac{m_e + m_h}{\hbar^2}\right)e^2F_0\,\Delta F\,L_z^4. \qquad \text{(B4)}$$

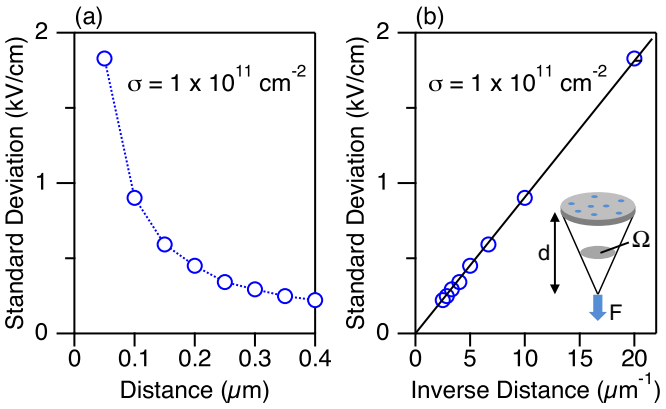


FIG. 9. (Color online) Numerical simulation of electric field fluctuation with a surface charge density $\sigma$ of $1 \times 10^{11}$ cm$^{-2}$ for different dot-surface distances $d$. The standard deviation of the field fluctuation is plotted (a) as a function of $d$, and (b) as a function of $d^{-1}$.

The above form reveals the $L_z$ dependence of line broadening, $\Delta E_S^X \propto L_z^4$.

## APPENDIX C: INFLUENCE OF DOT-SURFACE DISTANCE ON ELECTRIC FIELD FLUCTUATION

Figure 9 shows numerical simulation of electric field fluctuation with a surface charge density $\sigma$ of $1 \times 10^{11}$ cm$^{-2}$ for different dot-surface distances $d$. The standard deviation of the field fluctuation is plotted as a function of $d$ in Fig. 9(a) and as a function of $d^{-1}$ in Fig. 9(b). The agreement of the $d^{-1}$ dependence with a straight line in Fig. 9(b) suggests that the field fluctuation magnitude $\Delta F$ decreases with, and inversely proportional to, $d$. This observation is attributed to the following reason. We assume that an electric field is dominantly induced by surface charges inside a surface segment covered by a solid angle $\Omega$ from the dot, see the inset in Fig. 9(b). The number of charges in the segment, denoted by $n$, is fluctuated around the average number $n_0 = \sigma\Omega d^2$. The fluctuating number of $n$ determines a fluctuating field $F \propto n/d^2$, and follows Poissonian statistics whose standard deviation is $\sqrt{n_0}$. We therefore obtain $\Delta F \propto \sqrt{n_0}/d^2 \propto \sqrt{\sigma}/d$.


[1] *Single Quantum Dots: Fundamentals, Applications and New Concepts*, edited by P. Michler, *Topics in Applied Physics* (Springer-Verlag, Berlin, Heidelberg, 2003); *Single Semiconductor Quantum Dots*, edited by , *NanoScience and Technology* (Springer-Verlag, Berlin, Heidelberg, 2009).

[2] S. A. Empedocles, D. J. Norris, and M. G. Bawendi, Photoluminescence spectroscopy of single CdSe nanocrystallite quantum dots, Phys. Rev. Lett. **77**, 3873 (1996). S. A. Empedocles and M. G. Bawendi, Influence of spectral diffusion on the line shapes of single CdSe nanocrystallite quantum dots, J. Chem. Phys. B **103**, 1826 (1999).

[3] S. A. Blanton, M. A. Hines, and P. Guyot-Sionnest, Photoluminescence wandering in single CdSe nanocrystals, Appl. Phys. Lett. **69**, 3905 (1996).

[4] J. Seufert, R. Weigand, G. Bacher, T. Kümmell, A. Forchel, K. Leonardi, and D. Hommel, Spectral diffusion of the exciton transition in a single self-organized quantum dot, Appl. Phys. Lett. **76**, 1872 (2000).

[5] V. Türck, S. Rodt, O. Stier, R. Heitz, R. Engelhardt, U. W. Pohl, D. Bimberg, and R. Steingrüber, Effect of random field fluctuations on excitonic transitions of individual CdSe quantum dots, Phys. Rev. B **61**, 9944 (2000).

[6] G. Sallen, A. Tribu, T. Aichele, R. André, L. Besombes, C. Bougerol, M. Richard, S. Tatarenko, K. Kheng, and J.-P. Poizat, Subnanosecond spectral diffusion measurement using photon correlation, Nat. Photon. **4**, 696 (2010); Subnanosecond spectral diffusion of a single quantum dot in a nanowire, Phys. Rev. B **84**, 041405 (2011).

[7] M. Abbarchi, T. Kuroda, T. Mano, M. Gurioli, and K. Sakoda, Bunched photon statistics of the spectrally diffusive photoluminescence of single self-assembled GaAs quantum dots, Phys. Rev. B **86**, 115330 (2012).

[8] A. V. Kuhlmann, J. Houel, A. Ludwig, L. Greuter, D. Reuter, A. D. Wieck, M. Poggio, and R. J. Warburton, Charge noise and spin noise in a semiconductor quantum device, Nat. Phys. **9**, 570 (2013).

[9] C. Matthiesen, M. J. Stanley, M. Hugues, E. Clarke, and M. Atatüre, Full counting statistics of quantum dot resonance fluorescence, Sci. Rep. **4**, 4911 (2014).

[10] A. Berthelot, I. Favero, G. Cassabois, C. Voisin, C. Delalande, P. Roussignol, R. Ferreira, and J. M. Gérard, Unconventional motional narrowing in the optical spectrum of a semiconductor quantum dot, Nat. Phys. **2**, 759 (2006).

[11] J. Houel, A. V. Kuhlmann, L. Greuter, F. Xue, M. Poggio, B. D. Gerardot, P. A. Dalgarno, A. Badolato, P. M. Petroff, A. Ludwig, D. Reuter, A. D. Wieck, and R. J. Warburton, Probing single-charge fluctuations at a GaAs/AlAs interface using laser spectroscopy on a nearby InGaAs quantum dot, Phys. Rev. Lett. **108**, 107401 (2012).

[12] M. Hauck, F. Seilmeier, S. E. Beavan, A. Badolato, P. M. Petroff, and A. Högele, Locating environmental charge impurities with confluent laser spectroscopy of multiple quantum dots, Phys. Rev. B **90**, 235306 (2014).

[13] C. F. Wang, A. Badolato, I. Wilson-Rae, P. M. Petroff, E. Hu, J. Urayama, and A. Imamoğlu, Optical properties of single InAs quantum dots in close proximity to surfaces, Appl. Phys. Lett. **85**, 3423 (2004).

[14] A. Majumdar, E. D. Kim, and J. Vučković, Effect of photogenerated carriers on the spectral diffusion of a quantum dot coupled to a photonic crystal cavity, Phys. Rev. B **84**, 195304 (2011).

[15] J. H. Prechtel, A. V. Kuhlmann, J. Houel, L. Greuter, A. Ludwig, D. Reuter, A. D. Wieck, and R. J. Warburton, Frequency-stabilized source of single photons from a solid-state qubit, Phys. Rev. X **3**, 041006 (2013).

[16] J. Hansom, C. H. H. Schulte, C. Matthiesen, M. J. Stanley, and M. Atatüre, Frequency stabilization of the zero-phonon line of a quantum dot via phonon-assisted active feedback, Appl. Phys. Lett. **105**, 172107 (2014).

[17] K. Watanabe, N. Koguchi, and Y. Gotoh, Fabrication of GaAs quantum dots by modified droplet epitaxy, Jpn. J. Appl. Phys. **39**, L79 (2000).

[18] T. Mano, M. Abbarchi, T. Kuroda, C. A. Mastrandrea, A. Vinattieri, S. Sanguinetti, K. Sakoda, and M. Gurioli, Ultranarrow emission from single GaAs self-assembled quantum dots grown by droplet epitaxy, Nanotechnol. **20**, 395601 (2009).

[19] T. Mano, T. Kuroda, S. Sanguinetti, T. Ochiai, T. Tateno, J. Kim, T. Noda, M. Kawabe, K. Sakoda, G. Kido, and N. Koguchi, Self-assembly of concentric quantum double rings, Nano Lett. **5**, 425 (2005); T. Kuroda, T. Mano, T. Ochiai, S. Sanguinetti, K. Sakoda, G. Kido, and N. Koguchi, Optical transitions in quantum ring complexes, Phys. Rev. B **72**, 205301 (2005).

[20] T. Belhadj, T. Kuroda, C.-M. Simon, T. Amand, T. Mano, K. Sakoda, N. Koguchi, X. Marie, and B. Urbaszek, Optically monitored nuclear spin dynamics in individual GaAs quantum dots grown by droplet epitaxy, Phys. Rev. B **78**, 205325 (2008).

[21] G. Sallen, S. Kunz, T. Amand, L. Bouet, T. Kuroda, T. Mano, D. Paget, O. Krebs, X. Marie, K. Sakoda, and B. Urbaszek, Nuclear magnetization in gallium arsenide quantum dots at zero magnetic field, Nat. Commun. **5**, 3268 (2014).

[22] M. Yoshita, T. Sasaki, M. Baba, and H. Akiyama, Application of solid immersion lens to high-spatial resolution photoluminescence imaging of GaAs quantum wells at low temperatures, Appl. Phys. Lett. **73**, 635 (1998).

[23] J. Bocquel, A. D. Giddings, T. Mano, T. J. Prosa, D. J. Larson, and P. M. Koenraad, Composition profiling of GaAs/AlGaAs quantum dots grown by droplet epitaxy, Appl. Phys. Lett. **105**, 153102 (2014).

[24] T. E. Schlesinger and T. Kuech, Determination of the interdiffusion of Al and Ga in undoped (Al,Ga)As/GaAs quantum wells, Appl. Phys. Lett. **49**, 519 (1986).

[25] M. Abbarchi, T. Kuroda, T. Mano, K. Sakoda, C. A. Mastrandrea, A. Vinattieri, M. Gurioli, and T. Tsuchiya, Energy renormalization of exciton complexes in GaAs quantum dots, Phys. Rev. B **82**, 201301(R) (2010).

[26] M. Abbarchi, F. Troiani, C. Mastrandrea, G. Goldoni, T. Kuroda, T. Mano, K. Sakoda, N. Koguchi, S. Sanguinetti, A. Vinattieri, and M. Gurioli, Spectral diffusion and line broadening in single self-assembled GaAs/AlGaAs quantum dot photoluminescence, Appl. Phys. Lett. **93**, 162101 (2008).

[27] C. Kindel, G. Callsen, S. Kako, T. Kawano, H. Oishi, G. Hönig, A. Schliwa, A. Hoffmann, and Y. Arakawa, Spectral diffusion in nitride quantum dots: Emission energy dependent linewidths broadening via giant built-in dipole moments, Phys. Status Solidi Rapid Res. Lett. **8**, 408 (2014).

[28] B. Urbaszek, X. Marie, T. Amand, O. Krebs, P. Voisin, P. Maletinsky, A. Högele, and A. Imamoglu, Nuclear spin physics in quantum dots: An optical investigation, Rev. Mod. Phys. **85**, 79 (2013).

[29] J. Bardeen, Surface states and rectification at a metal semiconductor contact, Phys. Rev. **71**, 717 (1947).

[30] Y. Nannichi, J.-F. Fan, H. Oigawa, and A. Koma, A model to explain the effective passivation of the GaAs surface by $(NH_4)_2S_x$ treatment, Jpn. J. Appl. Phys. **27**, L2367 (1988).

[31] P. Y. Yu and M. Cardona, Fundamentals of Semiconductors, (Springer-Verlag, Berlin, Heidelberg, 2010), Chap. 8.3.

[32] E. Yablonovitch, C. J. Sandroff, R. Bhat, and T. Gmitter, Nearly ideal electronic properties of sulfide coated GaAs surfaces, Appl. Phys. Lett. **51**, 439 (1987).

[33] M. Xu, Y. Q. Wu, O. Koybasi, T. Shen, and P. D. Ye, Metal-oxide-semiconductor field-effect transistors on GaAs (111)A surface with atomic-layer-deposited $Al_2O_3$ as gate dielectrics, Appl. Phys. Lett. **94**, 212104 (2009).

[34] T. Mano, M. Abbarchi, T. Kuroda, B. McSkimming, A. Ohtake, K. Mitsuishi, and K. Sakoda, Self-assembly of symmetric GaAs quantum dots on (111)A substrates: Suppression of fine-structure splitting, Appl. Phys. Express **3**, 065203 (2010); T. Kuroda, T. Mano, N. Ha, H. Nakajima, H. Kumano, B. Urbaszek, M. Jo, M. Abbarchi, Y. Sakuma, K. Sakoda, I.

Suemune, X. Marie, and T. Amand, Symmetric quantum dots as efficient sources of highly entangled photons: Violation of Bell's inequality without spectral and temporal filtering, Phys. Rev. B **88**, 041306 (2013).

[35] N. Ha, X. Liu, T. Mano, T. Kuroda, K. Mitsuishi, A. Castellano, S. Sanguinetti, T. Noda, Y. Sakuma, and K. Sakoda, Droplet epitaxial growth of highly symmetric quantum dots emitting at telecommunication wavelengths on InP(111)A, Appl. Phys. Lett. **104**, 143106 (2014); X. Liu, N. Ha, H. Nakajima, T. Mano, T. Kuroda, B. Urbaszek, H. Kumano, I. Suemune, Y. Sakuma, and K. Sakoda, Vanishing fine-structure splittings in telecommunication-wavelength quantum dots grown on (111)A surfaces by droplet epitaxy, Phys. Rev. B **90**, 081301 (2014).

[36] J. Robertson, Y. Guo, and L. Lin, Defect state passivation at III-V oxide interfaces for complementary metal-oxide-semiconductor devices, J. Appl. Phys. **117**, 112806 (2015).

[37] S. Bietti, J. Bocquel, S. Adorno, T. Mano, J. G. Keizer, P. M. Koenraad, and S. Sanguinetti, Precise shape engineering of epitaxial quantum dots by growth kinetics, Phys. Rev. B (to be published).

[38] D. J. Griffiths, *Introduction to Quantum Mechanics*, 2nd ed. (Pearson Prentice Hall, Upper Saddle River, NJ, 2004).